phys. stat. sol. (a) **147**, 515 (1995)

Subject classification: 72.15 and 74.70; 68.70; S1.3

Institut für Metallkunde und Metallphysik
der Rheinisch-Westfälischen Technischen Hochschule Aachen[1])

Experimental Investigation and Simulation of the Normal Conducting Properties of a Heavily Cold Rolled Cu–20 Mass%Nb in situ Composite

By

U. HANGEN and D. RAABE

A fibre reinforced in situ metal matrix composite (MMC) consisting of Cu and 20 mass% Nb is manufactured by large strain cold rolling. The microstructure of the composite is investigated by means of optical and electron microscopy. The normal conducting properties of the MMC sheets in the presence of external magnetic fields are studied and compared to the electromagnetic behaviour of pure Cu and Nb sheets. The findings are discussed in terms of the microstructural changes which take place during rolling deformation. The resistivity of the MMC is simulated by assuming inelastic scattering of the condution electrons at the internal phase boundaries. Both, experiment and simulation, substantiate that the amount of internal boundaries and the filament spacing have considerable influence on the normal conducting properties of Cu–20 mass% Nb.

Ein faserverstärkter in situ Verbundwerkstoff mit metallischer Matrix (MMC) aus Cu und 20 Gew% Nb wird durch Kaltwalzen bis zu hohen Umformgraden hergestellt. Die Mikrostruktur der Verbundwerkstoffproben wurde mit Hilfe licht- und elektronenoptischer Mikroskopie untersucht. Die normalleitenden Eigenschaften des gewalzten Verbundwerkstoffes werden unter dem Einfluß äußerer magnetischer Felder gemessen und mit den elektromagnetischen Eigenschaften reiner Cu- und Nb-Bleche verglichen. Die Diskussion der ermittelten Daten erfolgt auf der Basis der mikrostrukturellen Entwicklung im Verlauf der Walzverformung. Der spezifische Widerstand des Verbundwerkstoffes wird unter der Annahme inelastischer Streuung der Leitungselektronen an den inneren Phasengrenzen simuliert. Sowohl die experimentellen Resultate als auch die Simulationen belegen, daß der Anteil an inneren Grenzflächen und der Faserabstand einen beträchtlichen Einfluß auf die normalleitenden Eigenschaften von Cu–20 Gew% Nb haben.

1. Introduction

Since Cu and Nb have negligible mutual solubility in the solid state [1, 2], fibre reinforced in situ metal matrix composites (MMCs) can be produced by large strain cold rolling of a cast ingot.

Binary systems of Cu with Ta, Cr, Mo, or V show a similar thermodynamical and mechanical behaviour as well as similar electrical properties in the normal conducting state (Fig. 1). However, they reveal significant limitations as compared to Cu–Nb. The densities of Ta, Cr, Mo, and V strongly deviate from that of Cu so that gravitational segregation during solidification deteriorates the potential of such alloys for technological applications. Furthermore, the melting temperatures of Ta and Mo are much higher than that of Nb which complicates the melting process.

[1]) Kopernikusstr. 14, D-52056 Aachen, Federal Republic of Germany.

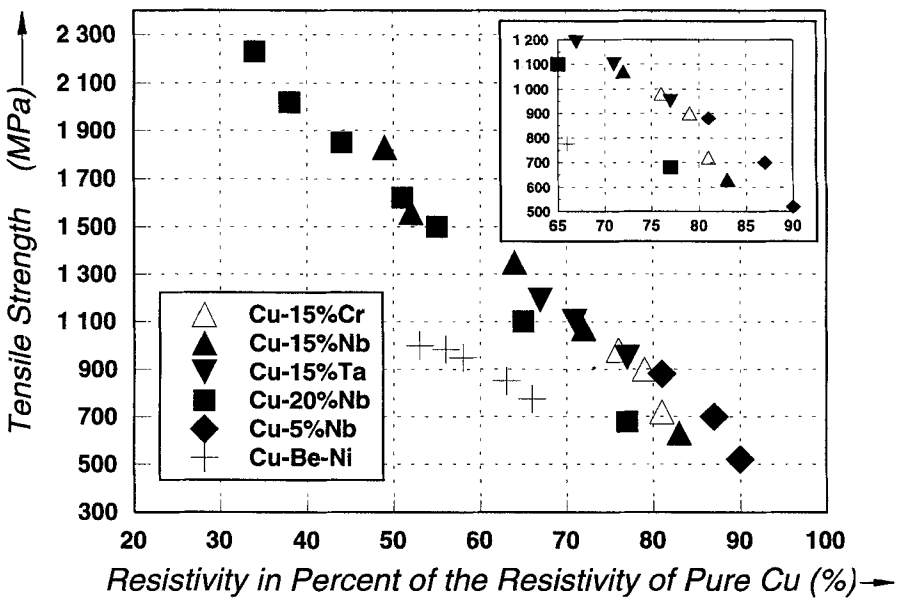

Fig. 1. Ultimate tensile strength vs. international annealed Cu standard, IACS, of various Cu-based alloys. Data taken from [3 to 14]

Cu and Nb reveal very similar densities (ϱ_{Cu} = 8890 kg/m^3, ϱ_{Nb} = 8580 kg/m^3). Therefore gravitational segregation does not occur, practically. Increased Nb content leads to a decrease of ductility, i.e. of elongation to fracture [3], and to a degradation of electrical conductivity [4]. An alloy with 20 mass% Nb content appears hence to combine optimum electrical and mechanical properties. Owing to their high tensile strength [5 to 7] and good electrical conductivity Cu–Nb composites have been under intensive investigation for the past 15 years. Although most of the studies have addressed the microstructure and thus the high tensile strength of Cu–20%Nb [3 to 17], an expanding body of literature has appeared on its electrical properties [18 to 23]. In this context especially wire drawn samples were investigated.

A quantitative correlation of microstructure and the resulting normal conducting properties of a heavily cold rolled Cu–Nb composite has, however, not yet been obtained. The current study is hence primarily concerned with the investigation of the electrical behaviour of a heavily cold rolled Cu–20% Nb composite in the presence of external magnetic fields and its correlation to microstructure. The results are compared to the electromagnetic behaviour of pure cold rolled Cu and Nb sheets.

2. Experimental

2.1 Manufacturing of the samples

The Cu and the Cu–20 mass% Nb alloy were melted in an induction furnace using a frequency of 10 kHz and a power of 30 kW [14]. The Cu and the Nb both had an initial purity of at least 99.99 mass%. Ingots of 18 mm diameter and 200 mm length were cast under an argon atmosphere at a pressure of about 0.8×10^5 Pa. Following the binary phase diagram [1] a temperature of at least 2025 K is required for melting a Cu–20 mass% Nb alloy. Other

authors [2], however, reported the occurrence of a miscibility gap in the liquid phase due to the presence of interstitial foreign atoms, such as O, N, H, and C. Hence a temperature of at least 2100 to 2120 K was employed in order to assure complete dissolution of the Nb. A crucible and a mould of high purity graphite were used. The mould was preheated to about 875 K to ensure good filling and fluidity. Details of the technique employed are explained elsewhere [14].

From the cylindrical ingot a block of $10 \times 15 \times 50\,\text{mm}^3$ was prepared. Strips of sheet material were produced by cold rolling to different degrees of deformation without intermediate annealing. Cold rolling was carried out up to a true strain of $\eta = 5.2$ ($\varepsilon = 99.5\%$), corresponding to a final sheet thickness of 60 μm.

2.2 Experimental techniques

For the investigation of the microstructure, scanning and transmission electron microscopy (SEM, TEM), as well as optical microscopy were employed. The initial dendrite size was directly measured on Nb dendrites which were isolated from the Cu matrix by etching the MMC in pure HNO_3. The measurements of the filament geometry were carried out on cross sections of the sheets.

The resistivity measurements were conducted by means of the dc four-probe technique using currents within the range 20 to 400 mA. for the investigation of the normal conducting properties (electrical resistivity and Hall constant) under externally imposed magnetic fields up to 20 T, an Oxford Instruments superconducting magnet as well as a Bitter magnet were used. The resistivity measurements were carried out within the temperature range 3 to 300 K. For the investigation of the Hall constant as a function of the true strain the external magnetic field was oriented parallel to the normal direction of the sheet. The Hall constant was investigated at a temperature of 4.2 K.

For each measurement a set of three cold rolled specimens, i.e. a Cu, a Nb, and a Cu–20 mass% Nb sheet having identical degree of deformation, were positioned in the centre of the magnets in such a way that the direction of the external magnetic field was perpendicular to the current flow in the strips and perpendicular to the normal direction (ND). The data were taken continuously during variation of the temperature or of the magnetic field. The cooling rate was controlled using a small heater, attached close to the specimens, and by addition of a He exchange gas. For the measurement of the temperature a carbon-glass resistance sensor was applied. The values of the voltage drop were averaged from measurements with opposite polarity using a frequency of 1 Hz. Within the temperature range 3 to 300 K about 1000 to 2000 data points were taken. In the corresponding diagrams merely a small fraction of the total data is shown owing to the use of discrete symbols. Errors due to thermal expansion and thermal nonequilibrium were neglected. The maximum error of the resistivity measurement was estimated to about 15%. The inaccuracy was attributed to the measurement of the specimen length which was to a certain extent inexact owing to the dimensions of the sodder points (1 mm).

3. Results

3.1 Microstructure

Fig. 2a shows the microstructure of the as-cast Cu–20 mass% Nb alloy. The primary Nb dendrites (dark) are embedded in the Cu matrix (light). After selectively dissolving the Cu matrix by use of HNO_3, metallography was carried out on the isolated dendrites (Fig. 2b).

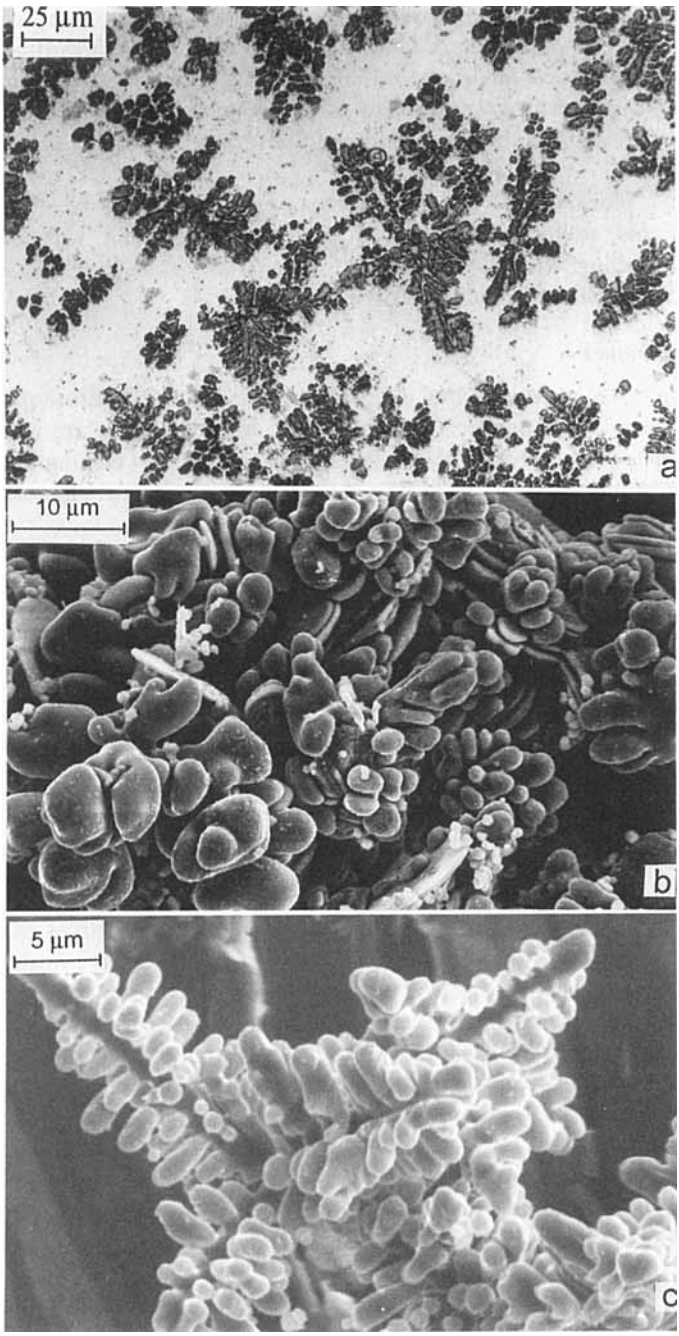

Fig. 2. SEM micrographs of as-cast Cu–20 mass% Nb, a) flat section, primary Nb dendrites (dark) embedded in the Cu matrix (light), b) isolated Nb dendrites, Cu matrix dissolved, c) isolated densely covered primary Nb dendrite branched out up to the third generation, Cu matrix dissolved

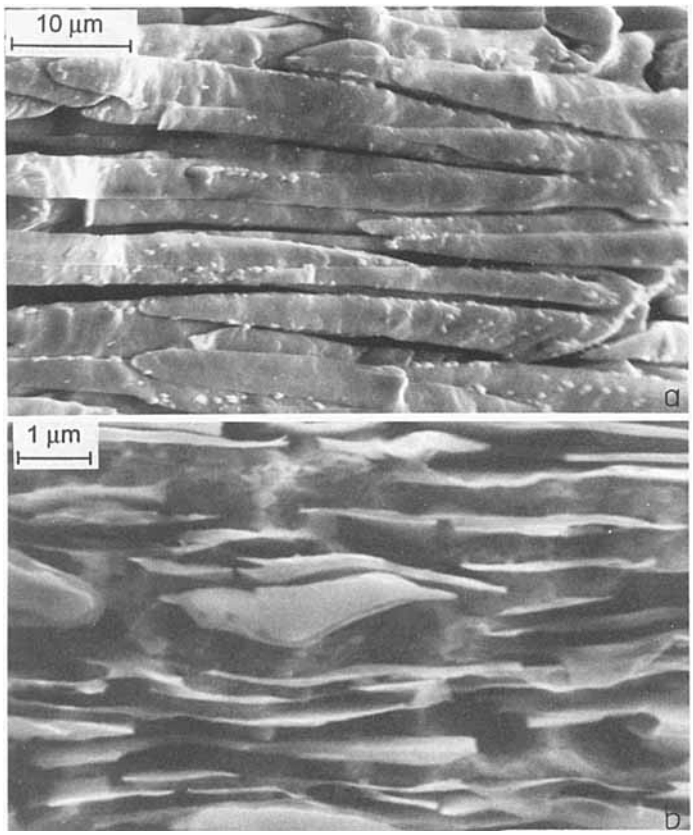

Fig. 3. SEM micrograph of the cold rolled Cu–20 mass% Nb composite, a) flat section of isolated Nb dendrites, Cu matrix dissolved, $\eta = 3$; $\varepsilon = 95\%$, b) cross section of the cold rolled sheet, $\eta = 5.2$; $\varepsilon = 99.5\%$

This technique allows to precisely account for the three-dimensional morphology of the Nb dendrites. The densely covered primary dendrites were seen to branch out up to the third generation (Fig. 2c). Whereas the orientations of the primary Nb dendrites were randomly distributed in the as-cast specimens the dendritic arms were commonly aligned parallel to the crystallographic $\langle 100 \rangle$ directions [12 to 14, 17]. In the as-cast state the mean diameter of the secondary dendrites, which are considered to have a large influence on the electrical and mechanical properties of the final MMC, was $d_0 = 2.2 \pm 0.4$ μm.

The evolution of the morphology of the Nb dendrites into elongated fibres is documented in Fig. 3a (flat section, $\eta = 3$; $\varepsilon = 95\%$) and Fig. 3b (cross section, $\eta = 5.2$; $\varepsilon = 99.5\%$). After small amounts of deformation the Nb morphology appeared quite inhomogeneous. Whereas some dendrite arms revealed considerable elongation, others appeared almost undeformed. In addition to that shear banding was observed to affect both, the deformation of the Cu matrix and of the Nb filaments. As is evident from Fig. 3b after heavy deformation the filaments revealed a more flattened shape but still an inhomogeneous thickness distribution. No shear bands were detected at this final stage of deformation. After the highest attained rolling deformation ($\eta = 5.2$; $\varepsilon = 99.5\%$) an average filament thick-

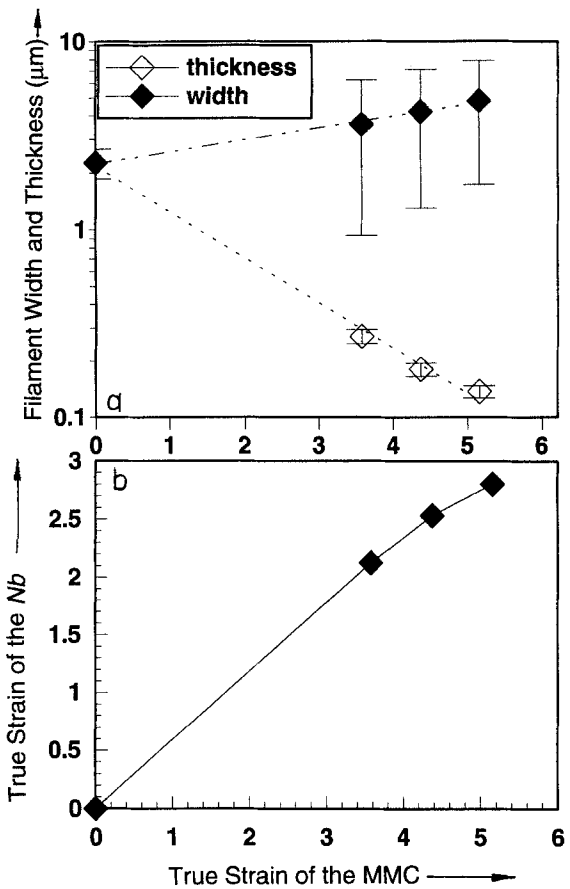

Fig. 4. Development of a) the filament width and thickness and b) the filament strain as a function of the true sheet strain

ness of about 130 nm and a filament spacing of about 500 nm was found. As is evident from Fig. 3a in the heavily deformed in situ MMC all filaments were aligned parallel to the sheet plane. The surface of the Nb filaments appears wavy and reminds of heavily deformed single crystals. The evolution of the filament thickness and width as a function of strain is given in Fig. 4a. The development of the true strain of the Nb filaments, as calculated from the metallographic data, is given as a function of the sheet deformation in Fig. 4b. The curve basically shows a linear dependence, although not a one to one correspondence. According to Fig. 4b, a sheet deformation of $\eta = 5.2$ ($\varepsilon = 99.5\%$) corresponds to a Nb filament deformation of $\eta = 3$ (95%). The actual deformation of the Nb phase was thus generally lower than expected for a homogeneous deformation of the sheet. If not explicitly stated otherwise, hereafter, η will be used to indicate the sheet deformation.

3.2 Electromagnetic properties

Measurements of the electrical normal state resistivity were conducted at three different temperatures. Fig. 5 shows the dependence of the resistivity of pure Cu, pure Nb, and of Cu–20 mass% Nb as a function of the sheet deformation at 295, 198, and 77 K. The resistivity

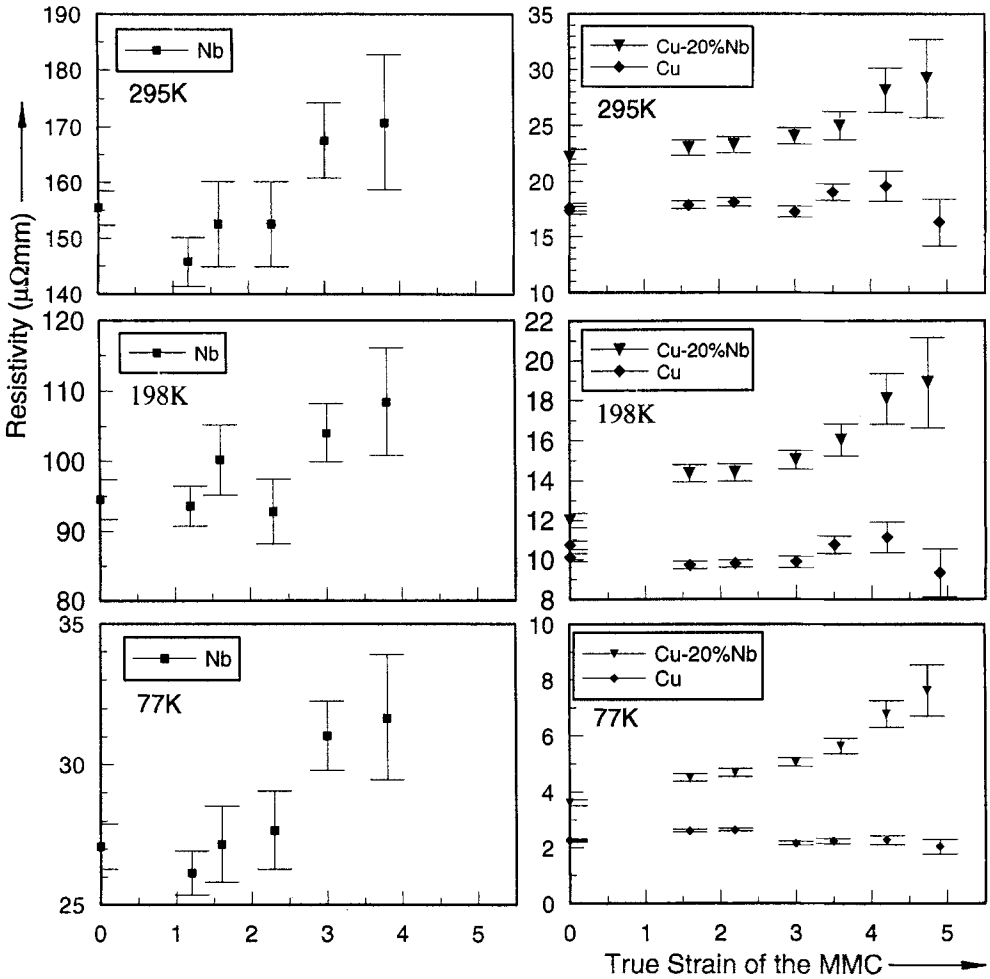

Fig. 5. Resistivity of cold rolled pure Nb, pure Cu and Cu–20 mass% Nb with progressing sheet deformation for three different temperatures

of pure Cu appears to be independent of the degree of deformation. The resistivity of Cu–20 mass% Nb and pure Nb is always larger than that of pure Cu and increases with the strain. In Fig. 6 the measurements of the annealed Cu–20 mass% Nb specimens (5 h at 823 K) are shown. It becomes apparent that the electrical resistivity of the MMC decreased notably upon annealing.

Fig. 7a presents the Hall constant as a function of the true strain. It is evident that the Hall constant and thus also the mobility of the electrons (Fig. 7b) decrease drastically with increasing strain. The Hall constant integrates the contribution of both, the Nb filaments and the Cu matrix. However, due to its higher volume fraction it is assumed that the main portion of the Hall voltage is contributed by the deflection of the conduction electrons in the Cu matrix.

In Fig. 8 the effect of deformation on the normal conducting properties and on the transition to the superconducting state is shown. It is revealed that not only the normal

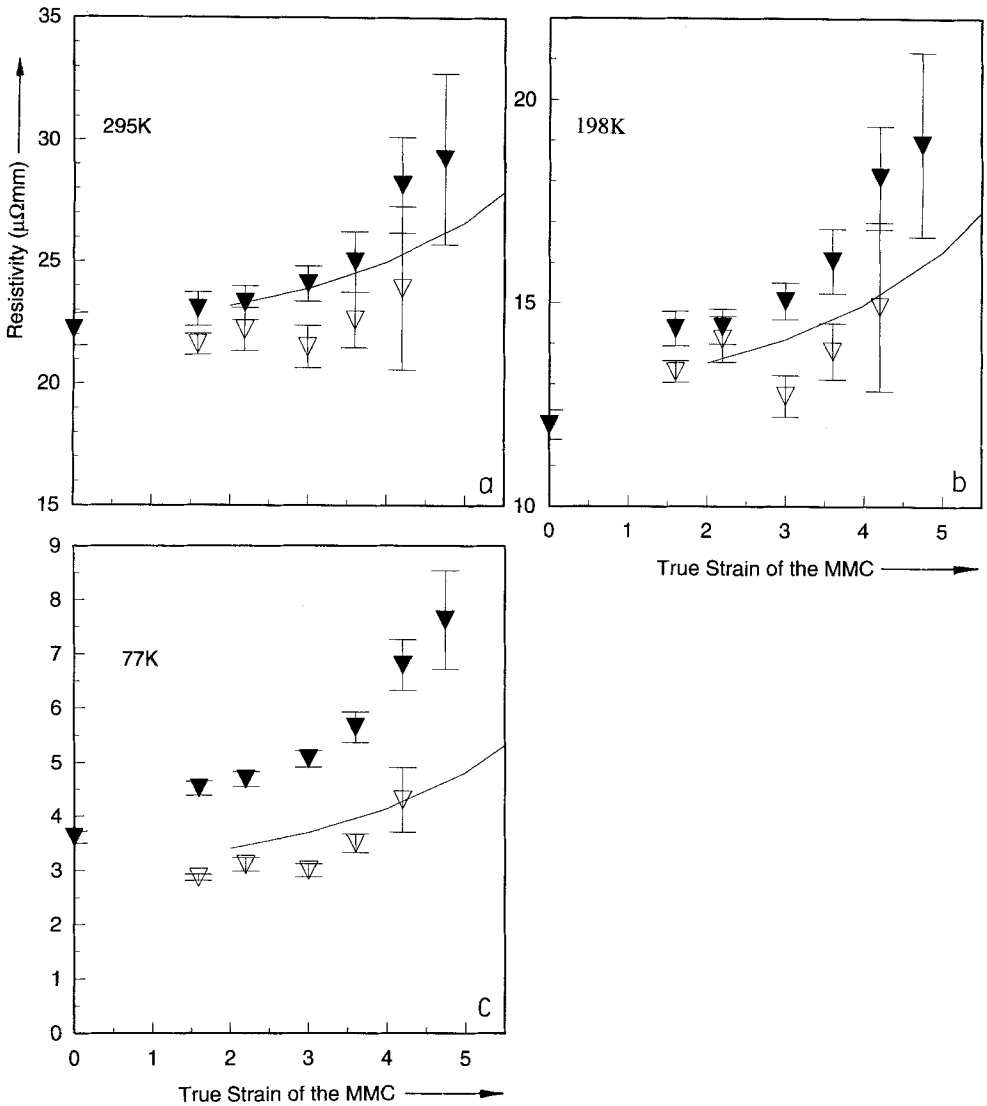

Fig. 6. Resistivity of Cu–20 mass% Nb with progressing sheet deformation measured at three different temperatures, with (▽) and without (▼) heat treatment (823 K, 5 h). The solid line shows the simulation of the electrical resistivity (cold rolled specimens). a) 295, b) 198, c) 77 K

state resistivity of Cu–20 mass% Nb but also the critical temperature which indicates the phase transition into the superconducting state considerably depend on the degree of deformation, i.e. on the microstructure. Both, with and without applied external magnetic field, the resistivity in the normal conducting state is higher and the critical temperature lower for the sample which had undergone a larger thickness reduction (Fig. 8).

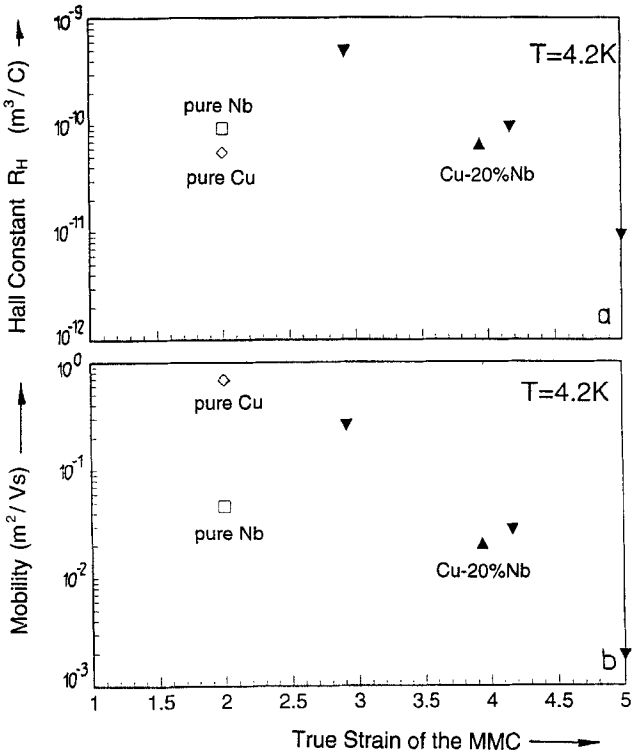

Fig. 7. a) Hall constant R_H and b) mobility of the electrons in pure Nb, pure Cu, and Cu–20 mass% Nb as a function of the true strain

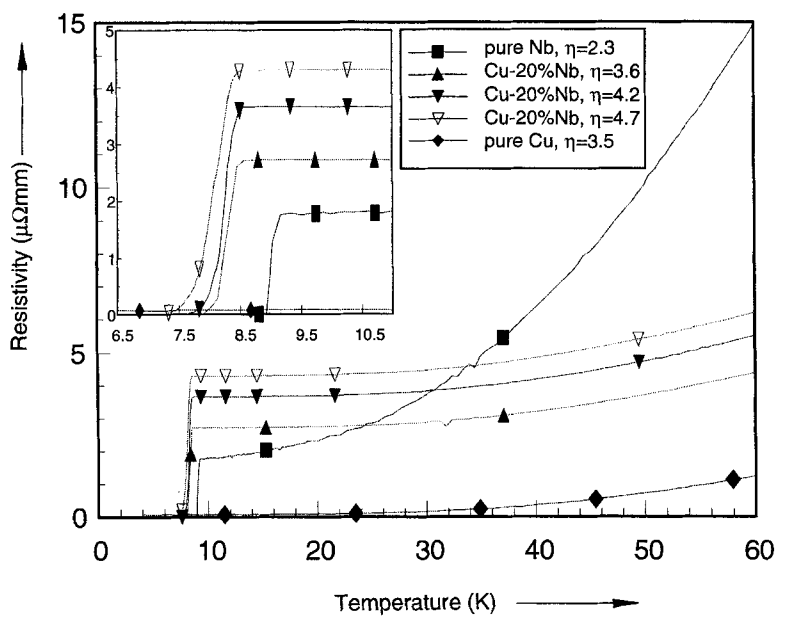

Fig. 8. Normal state resistivity (pure Cu) and transition to the superconducting state (pure Nb, Cu–20 mass% Nb) at low temperatures

4. Discussion

4.1 Microstructure

Cu and Nb have a negligible mutual solubility in the solid state. In the as-cast condition the Nb phase thus reveals a dendritic morphology (Fig. 2). The average diameter of the secondary dendrites is about 2 μm. Compared to other production methods this value is quite small [8, 10, 14] and thus ensures a high tensile strength after heavy deformation [12, 13].

The Nb morphology observed is inhomogeneous up to the highest attained deformation degree of $\eta \approx 5.2$ (Fig. 3b). This is due to several reasons. Firstly, it is assumed that the shear strains are inhomogeneously distributed in the rolled specimen. This is documented by the occurrence of shear bands at low and medium strains. Secondly, texture investigations show [15 to 17, 21] that at small strains initially randomly oriented Nb dendrites start to rotate until they are arranged parallel to the sheet plane. After this alignment ($\eta \approx 2$) a massive cross sectional area reduction of the dendrites was observed. However, those dendrites which were initially arranged parallel to the sheet surface in the as-cast specimen are flattened already in the early plastic regime. Thirdly, the deformation is strongly influenced by the incompatibility of the deformation of the f.c.c. (face centred cubic) Cu and the b.c.c. (body centred cubic) Nb. Since the distribution of the Nb phase is inhomogeneous, the Cu matrix which represents the softer phase has to undergo a higher deformation locally. This again modifies the local stress distribution within the sheet, i.e. neither the actual Cu deformation nor the actual Nb deformation equals the true strain of the sheet.

The wavy appearance of the surface of the flat cold rolled Nb dendrites (Fig. 3a) is attributed to the fact that b.c.c. grains which have a crystallographic $\{001\}\langle 110\rangle$ orientation can be deformed by activation of only two symmetric slip systems. As was shown by quantitative texture analysis [15, 16] the $\{001\}\langle 110\rangle$ orientation is indeed the dominant texture component of heavily cold rolled Cu–20 mass% Nb. This leads to a concentration of slip and consequently to the formation of large slip steps on the surface of the flat dendrites.

4.2 Electromagnetic properties

The electrical resistivity of a metal arises from the scattering of conduction electrons at static and dynamic lattice defects. Solute atoms like Cr, S, P and in particular the ferromagnetic elements Fe, Ni, Co considerably increase the eletrical resistivity. In comparison, the contribution of dislocations is relatively low even at large strains [24]. With increasing content of a second phase or with decreasing dimensions of the constituents the scattering of electrons at phase boundaries substantially degrades the electrical normal state conduction properties of the material.

The fact that the resistivity of pure Cu appears virtually unaffected by deformation (Fig. 5) is not surprising. Since only the cores of the dislocations add to the electrical resistivity, but contribute only a very small resistivity change per unit length of a dislocation, the dc four-probe technique applied is not accurate enough for measuring this change. Even for a dislocation density of $10^{16}\ m^{-2}$ the increase of electrical resistivity would amount only $\approx 0.2\ \mu\Omega$ mm [24]. Furthermore, various authors [7, 9, 15 to 17] reported the occurrence of dynamic recrystallization in the Cu matrix at large strains. It is thus assumed that a very high dislocation density is not reached even after large macroscopical strains.

The increase of the resistivity of Cu–20 mass% Nb at large strains, $\eta = 3$ (Fig. 5), has to be attributed to the inelastic scattering of the conduction electrons at internal phase boundaries. Very high degrees of deformation lead to an extraordinary increase of the amount of Cu–Nb boundaries. If the filament spacing between two phase boundaries reaches the order of magnitude of the mean free path of a conduction electron, a remarkable drop in conductivity can be expected. According to the present results a filament spacing in the order of 500 nm and a filament thickness of 130 nm can be achieved after the highest attained deformation of $\eta = 5.2$. Compared to the inelastic scattering at the phase boundaries the impact of the dislocations on the resistivity can be neglected [23, 25]. On the basis of the current microstructural results the loss of the electrical conductivity with increasing MMC deformation can now be treated more quantitatively.

For assessing the dependence of the normal state resistivity of the deformed MMC upon fibre geometry, the theory of inelastic electron scattering at the surface of very thin films [26, 27] was applied. However, in the current model the surface is replaced by the Cu–Nb phase boundary. It is stipulated that the two phases behave like two linear resistors connected parallel, the resistivity of each varies according to their filament thickness. The total resistivity of the MMC, ϱ, can then be regarded as the sum of the volumetrically weighted average of the resistivities of the individual pure phases, ϱ_{Cu} and ϱ_{Nb}, $\varrho = (0.8/\varrho_{Cu} + 0.2/\varrho_{Nb})^{-1}$. The Nb filament spacing is identified with the thickness of the Cu filaments. Both data are available from experiment. The resistivity of each phase can then be determined according to the equation of Dingle [25, 26], $\varrho(d) = \varrho_0(1 + 0.75(1 - p)(l_0/d))$, where $\varrho(d)$ is the resistivity as a function of the filament thickness, ϱ_0 the resistivity of a filament with infinite thickness, $(1 - p)$ the probability of inelastic scattering, l_0 the mean free path of the conduction electrons, and d the thickness of the filament. According to investigations on Cu–Nb it was estimated that $(1 - p)$ is close to 1 [23, 25, 28]. According to Dingle [26] this approach is valid for $d > l_0$. This condition holds for both, Cu ($d/l_0 \approx 11$) and Nb ($d/l_0 \approx 42$) corresponding to the current data for $\eta = 5.2$ and $T = 295$ K. The mean free path of a conduction electron in pure Cu was estimated theoretically [24] and confirmed experimentally [28, 29] as $l = 43$ to 45 nm at 293 K, $l = 61$ to 63 nm at 198 K, and $l = 138$ to 145 nm at 77 K. In pure Nb $l = 3.1$ nm at 293 K, $l = 5$ nm at 198 K, and $l = 17.6$ nm at 77 K were calculated on the basis of experimental data of Auer and Ullmaier [30]. The resistivities of both constituents can then be expressed as a function of fibre diameter and temperature. For the pure and undeformed constituents, Cu and Nb, the following resistivities were measured on bulk samples, $\varrho_{Cu0} = 17$ μΩ mm and $\varrho_{Nb0} = 155$ μΩ mm at 295 K, $\varrho_{Cu0} = 10$ μΩ mm and $\varrho_{Nb0} = 95$ μΩ mm at 198 K, as well as $\varrho_{Cu0} = 3$ μΩ mm and $\varrho_{Nb0} = 27$ μΩ mm at 77 K. The evolution of the filament thickness as a function of the strain was fitted from experimental data.

The results of the simulations are together with the experimentally detected resistivities depicted in Fig. 6 for the three different temperatures investigated. The evolution of the resistivity, i.e. especially the experimentally observed increase at large strains is adequately covered by the model. As a result the increase of resistivity in largely strained MMCs can essentially be attributed to scattering of conduction electrons at phase boundaries. However, it becomes apparent that especially at 198 K (Fig. 6b) and 77 K (Fig. 6c) the simulated data are somewhat too low and thus reveal a better agreement with the resistivities of the annealed specimens. This deviation is attributed to the microstructural data which the current simulation is based upon. It was shown by Verhoeven et al. [31] that transmission electron microscopy (TEM) has to be employed in order to painstakingly record filament

diameter and spacing also for heavily deformed Cu–Nb MMCs. It has thus to be taken into account that the experimentally observed average fibre data used for the fit procedure in the current work, are somewhat too large. Furthermore the real morphology and thus also the true amount of the phase boundaries is much more intricate than suggested by the here employed simplified fitting parameters.

This geometrical argument explains the good correspondence between the simulation and the experimental data of the annealed specimens. For the diffusion controlled coarsening of the Nb ribbons, mass transport can take place along the internal phase boundaries, with a much lower energy of activation than for bulk diffusion. Hence, in accord with experimental results [32] and theoretical estimations [33] a coarsening of the Nb filaments must be considered at temperatures exceeding 620 K. Such a two-stage coarsening of filaments is a frequently encountered mechanism observed during annealing of fibre reinforced MMCs [33]. During the first coarsening stage the initially curled Nb filaments form into fibres with a circular cross section to quickly reduce the interface area. Subsequently, Ostwald ripening takes place. In the current case (823 K, 5 h) it appears likely that only the first coarsening stage must be taken into account. Both, the evolution of the deformed and of the deformed and annealed specimens, correponds to similar findings on wire drawn Cu–20 mass% Nb MMCs [23, 25].

As is evident from Fig. 7a, the Hall coefficient of the composite reveals a strong dependence of the degree of deformation. At 4.2 K the Hall constant of pure Nb amounts to $R_H^{Nb} = 9.3 \times 10^{-11}$ m^3/C and that of pure Cu to $R_H^{Cu} = 5.5 \times 10^{-11}$ m^3/C. These values correspond to data reported by other authors [34]. Stipulating that the value of the Hall constant observed is essentially determined by the conduction electrons of the matrix phase their mobility can be calculated. From Fig. 7b it becomes apparent that the mobility decreases drastically with increasing strain. This observation can be interpreted in terms of inelastic scattering of the conduction electrons at internal boundaries since at large strains the average filament spacing is of the order of the mean free electron path in the Cu matrix. The measurement of the Hall constant represents a useful experiment to complement the investigation of the normal state resistivity. The investigation showed that by combining both results one can differentiate between the concentration and the mobility of conduction electrons.

5. Conclusions

The normal conducting properties of in situ manufactured Cu–20 mass% Nb composites were investigated and discussed in terms of the microstructure evolution during large strain cold rolling. The results were compared to the behaviour of the pure constituents. The electrical normal state resistivity of the composite was found to increase with decreasing fibre diameter and filament spacing. This was attributed to the inelastic scattering of the conduction electrons at Cu–Nb phase boundaries. The increase of the contribution of scattering at the internal boundaries with decreasing temperature was interpreted by the growing mean free path of the conduction electrons. The experimental data observed were compared to simulations which were conducted by stipulating inelastic scattering of conduction electrons at internal phase boundaries as dominant mechanism. The experimental data revealed a good agreement with the simulations and with similar findings on wire drawn Cu–Nb composites.

Acknowledgements

The authors gratefully acknowledge the kind support by the National High Magnetic Field Laboratory in Tallahassee, Florida, where the measurements of the electromagnetic properties were carried out. A portion of this work was supported by NSF Cooperative Agreement No. DMR-9016241 and by the State of Florida. The authors gratefully acknowledge the kind support by Dr. H.-J. Scheider-Muntau, Dr. L. T. Summers, and Dr. E. Palm. One of the authors gratefully acknowledges the kind support by the Adolf-Martens-Gesellschaft in Berlin, especially by Prof. Dr. Dr. e.h. W. Dahl and Prof. Dr. Dr. h.c. H. Czichos.

References

[1] D. J. CHAKRABATI and D. E. LAUGHLIN, Bull. Alloy Phase Diagrams **2**, 936 (1982).
[2] G. I. TEREKHOV and L. N. ALEKSANDROVA, Izv. Akad. Nauk SSR, Ser. Met. **4**, 210 (1984).
[3] G. FROMMEYER, Verbundwerkstoffe, DGM-Verlag, 1981 (p. 5).
[4] K. R. KARASEK and J. BEVK, J. appl. Phys. **52**, 1370 (1981).
[5] J. BEVK, J. P. HARBISON, and J. L. BELL, J. appl. Phys. **49**, 6031 (1978).
[6] J. BEVK and K. R. KARASEK, in: New Developments and Applications in Composites, Ed. D. KUHLMANN-WILSDORF and W. C. HARRIGAN, AIME, Warrendale (PA) 1979 (p. 101).
[7] W. A. SPITZIG, A. R. PELTON, and F. C. LAABS, Acta metall. **35**, 2472 (1987).
[8] W. A. SPITZIG, Acta metall. **39**, 1085 (1991).
[9] C. TRYBUS and W. A. SPITZIG, Acta metall. **37**, 1971 (1989).
[10] P. D. FUNKENBUSCH and T. H. COURTNEY, Acta metall. **33**, 913 (1985).
[11] W. A. SPITZIG and P. KROTZ, Scripta metall. **21**, 1143 (1987).
[12] D. RAABE and U. HANGEN, Proc. 15th Risø Internat. Symp. Mat. Sci.; Topic: Numerical Prediction of Def. Proc. and the Behaviour of Real Mat., Eds. S. I. ANDERSEN, J. B. BILDE-SORENSEN, T. LORENTZEN, O. B. PEDERSEN, and N. J. SORENSEN, Risø Nat. Lab., Roskilde (Denmark) 1994 (p. 487).
[13] D. RAABE, U. HANGEN, and G. GOTTSTEIN, Proc. Internat. Workshop High-Strength, High-Conduct. Composite Mat., Nat. High Magn. Field Lab., Tallahassee (Florida) 1994.
[14] F. HERINGHAUS, D. RAABE, L. KAUL, and G. GOTTSTEIN, Metall **6**, 558 (1993).
[15] D. RAABE and G. GOTTSTEIN, J. Physique (IV), C7, Suppl. J. Physique (III) **3**, 1727 (1993).
[16] D. RAABE, J. BALL, and G. GOTTSTEIN, Scripta metall. **27**, 211 (1992).
[17] F. HERINGHAUS, U. HANGEN, D. RAABE, and G. GOTTSTEIN, Mater. Sci. Forum **157/162**, 709 (1994).
[18] F. HERLACH, IEEE Trans. Magnetics **24**, 1049 (1988).
[19] J. D. EMBURY, M. A. HILL, W. A. SPITZIG, and Y. SAKAI, MRS Bull. **8**, 57 (1993).
[20] H.-J. SCHNEIDER-MUNTAU, IEEE Trans. Magnetics **18**, 32 (1982).
[21] F. HERINGHAUS, D. RAABE, and G. GOTTSTEIN, Metall **48**, 287 (1994).
[22] D. RAABE and F. HERINGHAUS, phys. stat. sol. (a) **142**, 473 (1994).
[23] F. HERINGHAUS, D. RAABE, and G. GOTTSTEIN, Acta metall., in press.
[24] J. G. RIDER and C. T. B. FOXON, Phil. Mag. **16**, 1133 (1967).
[25] D. RAABE, Computer Mater. Sci., in press.
[26] R. B. DINGLE, Proc. Soc. London Ser. 201, 1950 (p. 545).
[27] E. H. SONDHEIMER, Adv. Phys. **1**, 1 (1952).
[28] G. FROMMEYER and W. WASSERMANN, phys. stat. sol. (a) **27**, 99 (1975).
[29] F. W. REYNOLDS and G. R. STILLWELL, Phys. Rev. **88**, 418 (1952).
[30] J. AUER and H. ULLMAIER, Phys. Rev. B **7**, 136 (1973).
[31] J. D. VERHOEVEN, W. A. SPITZIG, F. A. SCHMIDT, P. D. KROTZ, and E. D. GIBSON, J. Mater. Sci. **24**, 1015 (1989).
[32] L. S. CHUMBLEY, H. L. DOWNING, W. A. SPITZIG, and J. D. VERHOEVEN, Mater. Sci. Engng. A **117**, 59 (1989).
[33] T. H. COURTNEY, in: New Developments and Applications in Composites, Ed. D. KUHLMANN-WILSDORF and W. C. HARRIGAN, AIME, Warrendale (PA) 1978 (p. 1).
[34] CH. KITTEL, Introduction to Solid State Physics, 6th ed., John Wiley and Sons, Inc., New York 1986.

(Received November 8, 1994)